Full Text View

Volume 28, Issue 10 (October 1998)

Journal of Physical Oceanography
Article: pp. 1946–1960 | Abstract | PDF (1006K)

Monsoon Response of the Sea around Sri Lanka: Generation of Thermal Domesand Anticyclonic Vortices

P. N. Vinayachandran* **and Toshio Yamagata**

Department of Earth and Planetary Physics, Graduate School of Science, University of Tokyo, Tokyo, Japan

(Manuscript received February 19, 1997, in final form December 11, 1997)

DOI: 10.1175/1520-0485(1998)028<1946:MROTSA>2.0.CO;2

ABSTRACT

Results from an ocean general circulation model are used to study the response of the oceanic region surrounding Sri Lanka to monsoonal winds. East of Sri Lanka, a cold dome (Sri Lanka dome, SLD) develops during the southwest monsoon (SWM) in response to cyclonic curl in the local wind field. The dome decays after September due to the arrival of a long Rossby wave, associated with the reflection of the spring Wyrtki jet at the eastern boundary of the ocean. East of the SLD an anticyclonic eddy exists that is in intermediate geostrophic (IG) balance. North of Sri Lanka a cold dome (Bay of Bengal dome) develops after the SWM associated with a cyclonic gyre forced by Ekman pumping. The source of cold water of the Bay of Bengal dome is traced back to the SLD and upwelling zone along the east coast of India. South of Sri Lanka a major part of the Southwest Monsoon Current (SMC) turns northeastward and flows into the Bay of Bengal. The part that flows eastward terminates at progressively western longitudes as the season progresses. This termination and the shallowness of the SMC is due to a Rossby wave generated near the eastern boundary by weakening of the spring Wyrtki jet and anticyclonic wind stress curl. This Rossby wave follows the one associated with the spring Wyrtki jet and has dominant velocities toward southwest. A large anticyclonic vortex, embedded in the SMC, results from the geostrophic adjustment process for the surface water converged by the long Rossby wave and the eastward zonal current. Energy analysis of this anticyclonic vortex as well as the IG eddy east of the SLD shows direct conversion from mean kinetic energy to eddy kinetic energy suggesting that barotropic instability is the mechanism that leads to eddy generation.

This study suggests two links that allow exchange between the Bay of Bengal and the rest of the Indian Ocean: The first is the SMC, which is an open ocean current, and the second is the equatorward East India Coastal Current during November–January, which is closely attached to the coast.

1. Introduction

The circulation along the coast of Sri Lanka (Fig. 1) is crucial for the interaction among the Arabian Sea, the Bay of Bengal, and the equatorial Indian Ocean. The monsoon current south of Sri Lanka is westward during the winter and eastward during the summer (Cutler and Swallow 1984). According to Schott et al. (1994) the circulation is particularly complex during the southwest monsoon (SWM) due to interaction of the eastward Southwest Monsoon Current (SMC) with a Rossby wave radiated from the eastern boundary. However, their study was limited to a meridional section along 80° 30′E and much of the current, especially its fate east of Sri Lanka, remains unexplored. Furthermore, the mechanisms that cause the observed variation of the SMC south of Sri Lanka, for instance, the occasional westward flow and the shallow structure, are not well understood. This is one motivation for this study.

The circulation of the Bay of Bengal undergoes dramatic seasonal variation, which has been well represented in the hydrographic observations in the western part of the bay. The best organized feature of the circulation is an anticyclonic gyre (Shetye et al. 1993) with a poleward East India Coastal Current (EICC) (Legeckis 1987). This pattern is present during February–April when the winds are weak but possess anticyclonic curl. The gyre disappears during the SWM; the EICC is southward in the northern part of the coast and northward in the southern part and the flow field consists of several rings (Shetye et al. 1991). During the northeast monsoon (NEM) the EICC flows southward along the entire coastline (Shetye et al. 1996). The seasonal cycle of the circulation in the open bay is still unclear. Hydrographic data suggest a northeastward flow during the SWM (Murthy et al. 1992) and a cyclonic gyre during early winter (Suryanarayana et al. 1993). The seasonal evolution of circulation in the bay has evoked considerable interest in the recent past (Potemra et al. 1991; Yu et al. 1991; McCreary et al. 1993, hereafter MKM;McCreary et al. 1996, hereafter MHSS; Shankar et al. 1996; Vinayachandran et al. 1996). The focus of these studies was on the seasonal cycle of circulation and its forcing mechanisms. In particular, MKM and MHSS examined the relative roles of remote forcing from the equator, remote effects from the eastern boundary of the Bay, Ekman pumping, and local alongshore winds on the EICC in great detail. The attention, however, was confined to the large-scale circulation particularly on the EICC (e.g., MKM, MHSS). Using an ocean general circulation model (OGCM) described in section 2, we show that the circulation in this region consists of several smaller-scale gyres.

Climatological thermal structure along 85°E (Fig. 2) shows that a well-developed dome is located east of Sri Lanka during July. A second dome, which is weaker than the first, is seen farther north during December (Fig. 3). We refer to the former as the Sri Lanka dome (SLD) and the latter as the Bay of Bengal dome (BBD). In this paper we study the seasonal evolution of these domes and the circulation around Sri Lanka, the SMC in particular, using an OGCM. The evolution of the SLD and BBD are described in sections 3 and 4, respectively. An anticyclonic eddy present in the model results during the SWM, east of the SLD, is described in section 5. The model SMC south of Sri Lanka is presented in section 6 and a summary is provided in section 7.

2. Model

The OGCM used in this study is an Indo–Pacific model adapted from the Geophysical Fluid Dynamics Laboratory ocean model (Cox 1984). A brief description of the model configuration should suffice here as a detailed account of the model setup has been presented earlier (Masumoto and Yamagata 1993; Masumoto and Yamagata 1996) where the simulated seasonal cycle in the seas around Indonesia was studied. The usefulness of this OGCM to investigate ocean dynamics and physics of the domes in particular has been demonstrated before (Umatani and Yamagata 1991; Masumoto and Yamagata 1991; Yamagata and Izuka 1995).

The model domain covers the Indian and Pacific Oceans between 50°S and 30°N. The grid spacing is a nominal 0.5° in both latitude and longitude. There are 20 levels in the vertical of which 8 are in the upper 100 m with a spacing of 10 m in the uppermost 5 levels. Bottom topography fitted into the model is from the ETOPO5 dataset. Sponge layers are introduced near the northern and southern walls in order to mitigate the effect of artificial walls. Lateral eddy viscosity and diffusivity are 2×10^7 and 1×10^7 cm^2 s^{-1} respectively and vertical eddy viscosity and diffusivity are parameterized using the Pacanowski and Philander (1981) scheme. The net surface heat flux (Q) is calculated using the formula

$$Q = Q_c + \lambda(T - T_c),$$

where T is the model temperature at 5 m (the uppermost level), T_c is the climatological sea surface temperature, Q_c is the climatological heat flux, and λ is the Newtonian damping term. Values of T_c, Q_c, and λ are taken from the Comprehensive Ocean–Atmosphere Data Set (Oberhuber 1988). In the Bay of Bengal λ has a mean value of −40 W m^{-2} K^{-1}. The model salinity is held constant at 35.0 psu. The model was started from the state of rest and annual mean temperature (Levitus 1982) and integrated for 5 years, forced by Hellerman and Rosenstein (1983) wind stress climatology multiplied by 0.75

(Stockdale et al. 1993). The results presented here are for the fifth year of model integration for the region shown in Fig. 1.

The simulated seasonal cycle of circulation (Fig. 4) agrees well with observations (Cutler and Swallow 1984). The large-scale features of the present simulations are remarkably similar to that in a 2.5-layer reduced gravity model of MKM and a linear continuously stratified model of MHSS. The difference is primarily in the presence of several gyres in our solution in the region between the equator and 10°N. The simulated upper-layer temperature (Fig. 5) is cooler than the climatology due to the limitations of the observed Q_c and λ as well as the parameterization of heat flux in the model.

3. The Sri Lanka dome

Figures 4 and 5 show the annual cycle of model currents and temperature respectively at a depth of 35 m. A cyclonic circulation pattern appears east of Sri Lanka during May, matures during July, and disappears in September. This result is consistent with ship drifts (Cutler and Swallow 1984), which show a southward current along the east coast of Sri Lanka during the SWM. Associated with this cyclonic circulation, a patch of cold water with temperature less than 25°C appears first during June. This patch attains a near-circular shape during July as seen in Fig. 5 and forms the core of the SLD. The western flank of the dome is a southward coastal current that flows against local winds. The SMC is on the southern flank. A northward flow, which moves westward with the progress of the SWM, is on the eastern flank. Comparison of the vertical section of model temperature along 85°E (Fig. 6) with the Levitus and Boyer (1994) climatology (Fig. 2) suggests that the model has captured the essential undulations of the isotherms associated with the evolution of the dome. The dome in the climatology is broader, smoother (perhaps due to averaging), and it is warmer than in the model result. The spreading of the thermocline north of 3°N is well captured by the model.

The genesis of the dome coincides with the existence of a strong cyclonic curl in the wind field east of Sri Lanka (Fig. 7), which peaks during May–September. The upward Ekman pumping induced by this cyclonic curl brings cooler water to the near-surface layers. This is seen in Fig. 8a, which shows the heat balance of SLD. The rate of change of heat content is negative during April–August, coinciding with the life cycle of the dome. The isolated patch of cold water (<24° C) during July (Fig. 5) suggests that upwelling of cold water is the major factor causing the negative heat content change. The major contribution to the heat content change, however, comes from lateral convergence (Fig. 8a). This is reasonable because cold water brought into the dome due to Ekman pumping leaves the box laterally near the surface. The advection of cold water upwelled along the east coast of India (Shetye et al. 1991) into the dome is unlikely since the currents are not favorable for this to occur until September. The decay of the dome begins during September. A strong northward flow east of Sri Lanka, which is separated from the coast by a southward current, replaces the cyclonic gyre. Consequently warm water advected from the east occupies the dome region, and the cold water patch moves northeast forming an eastward tongue (Fig. 5).

Figure 8b shows the vertical velocity from the model (w) at 107 m, the Ekman pumping (w_{Ek}), and the difference between the two ($w_{rem} = w - w_{Ek}$). At the base of the Ekman layer, since the vertical variation of the model vertical velocity is small, w_{rem} may be considered as the effect of remote forcing. This definition of remote forcing includes Rossby waves generated to the east of the box by Ekman pumping as well as Kelvin waves along the eastern boundary (see MHSS for a discussion of each factor separately). During the May–July period the dominance of Ekman pumping is clearly seen. Therefore, formation of the dome is certainly linked to the strong cyclonic curl in the wind stress over the dome (Fig. 7). Though the wind stress curl remains positive through December, the downwelling due to the arrival of a warm Rossby wave from the east causes the decay of the dome. The sloping contours in Fig. 9 suggest that this Rossby wave originates from the eastern boundary and it is strengthened by the local wind stress curl as it propagates westward. These are consistent with the findings by MHSS in their linear model.

4. The Bay of Bengal dome

A cyclonic gyre forms in the southwestern bay during September and survives through January. The western rim of this gyre is the equatorward EICC of the NEM (Shetye et al. 1996). This gyre is confined to the west of 90°E longitude and to the south of 20°N latitude during December and January. A single dataset that shows the presence of the complete cyclonic gyre does not exist. Ship drifts (Cutler and Swallow 1984) and hydrography (Shetye et al. 1996) clearly demonstrate the presence of the southward EICC. There are indications of the northern branch of the gyre in the hydrographic observations (Shetye et al. 1996). Dynamic topography calculated from climatological (Levitus and Boyer 1994; Levitus et al. 1994) data shows a cyclonic circulation in the western bay after the SWM, which tends to be confined to the southwestern Bay during January (Fig. 10) as in the model results. The center of this cyclonic gyre has waters cooler by about 2°C (Fig. 5) than the surroundings and may be called the Bay of Bengal dome. The BBD is shallower (Fig. 11) than the SLD but is spread over a much larger area. The BBD in the climatology (Fig. 2) is smoother and covers a much larger area than in the model.

MHSS found that the formation of the cyclonic gyre in their numerical model is in response to the positive Ekman pumping in the bay (Fig. 7). In their solution the cyclonic gyre located east of Sri Lanka during the SWM moved northward (see Fig. 5d of MHSS) suggesting a dynamic link between SLD and BBD. Our solution suggests that a cyclonic circulation develops independently during September (Fig. 4). Figure 12 shows that this cyclonic circulation is forced by the Ekman pumping within the BBD. The cyclonic gyre is well developed by November and weakens after December following the change in Ekman pumping. Figure 12 also suggests that remote effects also contribute to the decay of BBD. This is consistent with the westward movement of the northeastward flow that forms the eastern arm of BBD during November–January. MHSS also suggests that remote forcing from the equator contributes to the decay of the BBD in a minor way.

The SLD has an important role in the thermodynamics of the BBD. Comparison of the model thermocline depth with climatology (Levitus and Boyer 1994) shows that the SLD moves northward during September. The cold water of the SLD that moves northward during September appears to be the major source of cold water in the BBD. This is accomplished by the circulation during the transition from the SWM to the NEM. Though the EICC (Fig. 4) is equatorward after September, its path around Sri Lanka into the Arabian Sea is not continuous before November. Ship drift climatology (Cutler and Swallow 1983) also supports this feature. Until then the water seems to recirculate into the bay through the northeastward current east of Sri Lanka collecting in the BBD (Figs. 4 and 5). Another source of cold water for the BBD is the SWM upwelling along the east coast of India (Shetye et al. 1991). Upwelling conditions prevail in the model results until September. Part of this upwelled cold water that moves southward (when the EICC is equatorward) and offshore remains within the cyclonic gyre due to the strong northeastward current east of Sri Lanka. Thus the BBD appears to be a sink of cold water upwelled in the surroundings during the SWM. The EICC during November does not cause significant decay of the dome as a large volume of cold water has moved away from the coast by then. The decay is efficient when the EICC reverses during spring and an anticyclonic gyre occupies the bay.

The heat balance of the BBD (Fig. 12) clearly demonstrates that lateral convergence, described above, is the largest contributor to the heat content change, especially during its formative stage. The warming of the dome due to convergence of warm water into the dome starts in December and accelerates in January. The heat gain from the atmosphere and warm water advection from the south (Legeckis 1987) also contribute to the warming. Upwelling within the BBD is weaker than in the SLD (Fig. 12b).

5. The intermediate geostrophic (IG) eddy east of the Sri Lanka dome

Model results during the SWM show the presence of an anticyclonic eddy east of the SLD, centered at 90°E (Fig. 4). It is not represented in the available datasets, probably due to its small size. The eddy is straddled by the northward current that marks the eastern boundary of the SLD and a southeastward flow east of 90°E. It is circular in shape with a radius of about 150 km and it is best developed in the upper mixed layer, which is about 50 m deep. Because of the shallow, distinct thermocline, it is reasonable to assume that the eddy can be described by a shallow water model in which the thickness of the upper layer (H) is 50 m. The temperature of the mixed layer is 28°C and that below the thermocline is 14°C giving a value of 0.04 m s^{-2} for the reduced gravity (g^*). This gives a propagation speed of 11.3 cm s^{-1} for linear nondispersive Rossby waves at 8°N. The phase speed calculated from the slope of the velocity contours (east of 86°E) in Fig. 9 is 12.4 cm s^{-1}, which is consistent with theory. The center of the eddy moves westward at a similar speed.

The three nondimensional parameters governing the shallow water equation on a β plane are the beta parameter ($\beta^* = \beta L/f$), Rossby number ($R^* = U/fL$), and stratification parameter ($s^* = a^2/L^2$) (Yamagata 1982; Williams and Yamagata 1984). Here f is the Coriolis parameter ($f = 2\Omega \sin\phi$) where ϕ is the latitude and Ω is the angular velocity of the rotation of the earth, β is the variation of f with latitude, L is the horizontal length scale, U is the nondimensional velocity, and a is the Rossby deformation radius ($a = (g^*H)^{1/2}/f$). For the eddy east of SLD the values of these parameters are $\beta^* = 0.2$, $R^* = 0.02$, and $s^* = 0.2$. These values satisfy the unique conditions $\beta^* < O(1)$, $s^* \sim S\beta^*$, and $R^* \sim E(\beta^*)^2$, where S and E are numbers of $O(1)$. Therefore, the eddy is certainly governed by the intermediate geostrophic dynamics (Williams and Yamagata 1984); the anticyclonic eddy is balanced by weak planetary wave dispersion and weakly nonlinear planetary geostrophic divergence.

To find out the mechanism that generates the eddy in the model we have calculated the mean kinetic energy (MKE), mean available potential energy (APE), eddy kinetic energy (EKE), eddy available potential energy (EPE), and the conversion rates using the formulation of Boning and Budich (1992). (Complete energy analysis is not attempted because it is beyond the scope of the paper and the focus here is on the eddy generation.) The mean and eddy components were calculated from the daily snapshots of the model output for the May–September period of the fifth model year. Figure 13a shows the result for the IG eddy. Direct conversion of MKE to EKE suggests that the eddy is generated by barotropic instability associated with barotropic energy transfer.

6. The Southwest Monsoon Current

The SMC south of Sri Lanka was believed to be an eastward zonal current during the SWM. Recent current meter mooring records (Schott et al. 1994) show that this current is often separated from the coast of Sri Lanka by a westward flow. During June the eastward model SMC is separated from the coast by a narrow westward current. The SMC extends to the equator in the south, merging with the equatorial jet and it extends to the eastern boundary in the east. East of Sri Lanka, the SMC branches into two: one branch turns northeastward to enter into the Bay of Bengal during the entire season and the other continues eastward (Fig. 4). The eastern branch terminates at progressively western longitudes with the progress of the SWM (Fig. 4): The zonal velocity component averaged between 2° and 6°N is westward east of 89°E, 85°E, and 83°E during July, August, and September, respectively. These model results are in good agreement with the ship drifts (Cutler and Swallow 1983) and geostrophic flow field (Fig. 14). Hydrographic observations in the open bay during the SWM of 1984 (Murthy et al. 1992) clearly show the presence of the northeastward flow. This evidence suggests that most of the SMC flows into the bay, establishing a link between the Bay of Bengal and the rest of the north Indian Ocean.

The most remarkable feature of the SMC is a large anticyclonic vortex south of Sri Lanka (Fig. 4). An eastward flow on the northern edge of the vortex and a westward flow on the southern edge has been noted by Schott et al. (1994, see their Figs. 4c and 4f). Their acoustic doppler current profiler measurements along 80°30′E during July 1993 show that the current south of about 2.5°N was mainly northward at 20 m and westward at 100 m. A current meter mooring at 4° 10.7′N also showed that the flow is occasionally westward during July and August. The vortex is present, albeit not so clearly, in the simulation of MKM; their result showed an eastward flow south of Sri Lanka and a westward flow just north of the equator. To build further confidence in the model result, we have analyzed the sea surface topography measured by a precision radar altimeter aboard the Ocean Topography Experimental satellite (TOPEX/Poseidon). The sea surface height anomaly (Tapley et al. 1994) shows that a high is located southeast of Sri Lanka, which supports the anticyclonic vortex simulated by the model (Fig. 15).

The dynamics in this region is strongly influenced by Rossby wave propagation. The spring Wyrtki (1973) jet excites an equatorial Kelvin wave, part of which propagates along the periphery of the bay as a coastal Kelvin wave. A Rossby wave radiated by this coastal Kelvin wave is seen south of Sri Lanka during the SWM. The velocity associated with this Rossby wave is northeastward. The arrival of this Rossby wave causes the northward migration of the SMC and the disappearance of westward flow south of Sri Lanka (Schott et al. 1994). Further, it appears that this Rossby wave is responsible for the intrusion of a major part of the SMC into the Bay of Bengal.

An interesting result from the present study is the propagation of a second Rossby wave signal. This Rossby wave associated with southwestward flow leaves the eastern boundary during June (Fig. 16). Both climatological data (Fig. 14) and TOPEX/Poseidon data (Fig. 15) are in good agreement with this result. The leading edge of this wave reaches south of Sri Lanka during July (Fig. 4). Possible mechanisms that can excite this Rossby wave are the weakening of the spring Wyrtki jet and the fairly large anticyclonic curl in the wind field over the eastern boundary region (Fig. 7). MHSS suggests that a major contribution comes from the former mechanism. This Rossby wave has three implications: 1) it causes the termination of the eastward SMC (Fig. 4), 2) it causes the SMC to be shallow (Fig. 17) as observed by Schott et al. (1994), and 3) it maintains the turning of the SMC into the Bay of Bengal (Fig. 4). Figure 18 shows the Ekman component of the surface flow calculated from the Hellerman and Rosenstein (1983) wind stress and surface geostrophic velocity calculated from Levitus and Boyer (1994) temperature and Levitus et al. (1994) salinity climatologies. The westward geostrophic flow dominates the eastward Ekman component east of about 90°E, which is consistent with the above results. In the west, as shown by Hastenrath and Greischar (1991), the Ekman component dominates.

The anticyclonic vortex south of Sri Lanka has a radius of about 500 km and is straddled by the two Rossby waves discussed above. The vortex appears first during June, matures into a near-circular shape during July, and deforms during August. The center of the vortex propagates westward at a speed of 13 cm s^{-1}. The propagation speed of the Rossby wave estimated from the slope of velocity contours in Fig. 16 is about 40 cm s^{-1}. At 3°N the upper-layer thickness is about 75 m giving a propagation speed of 121 cm s^{-1} for the linear nondispersive Rossby waves in a reduced gravity model. Thus, the westward propagation of the Rossby wave is much smaller than the theoretical value. MKM also found a similar difference in the phase speeds. Reduction of the westward propagation speed is possible due to active wave–mean flow interaction in the presence of an eastward current (Greatbatch 1985). Therefore, it is reasonable to conclude that in the presence of the eastward SMC the Rossby wave travels slower. The nonlinear parameters (see section 5) for this eddy are evaluated to be $\beta^* = 1.5$, $R^* = 0.06$, and $s^* = 0.21$, suggesting that the IG dynamics is not applicable, mainly due to its proximity to the equator. On the other hand the dynamics is closer to the planetary geostrophic regime (Williams and Yamagata 1984; Williams and Wilson 1988). The energy analysis (Fig. 13b) suggests that barotropic instability is the mechanism that leads to eddy formation.

Greatbatch (1985) found that a Rossby wave, when it propagates westward against a zonal current, breaks into several vortices. The pattern seen here is remarkably similar to that simulated by Greatbatch (see his Fig. 4). Thus it appears that the vortex is generated due to the modification of the Rossby wave propagation by the eastward SMC. Rossby wave reflection caused by the Wyrtki jet takes place south of the equator as well, but a vortex does not form there, which

supports our argument that the eastward SMC is essential for the formation of the vortex. It may be recalled that blocking of the wave propagation by the zonal current is crucial to the stability of the vortex and a westward flow between an eastward equatorial jet and eastward low-latitude current further stabilize the vortex (Williams and Wilson 1988). The westward flow associated with the second Rossby wave signal between SMC and the eastward flow at the equator may provide a similar scenario.

7. Summary

In this paper results from an Indo–Pacific OGCM are used to study the response of the sea around Sri Lanka to the SWM. The results are compared with available observations and are explained in the light of previous theoretical investigations. The role of gyres of the order of few hundred kilometers in modifying the thermal structure of the upper ocean is significant; the SLD and the BBD maintain waters cooler by 2°–3°C than the surroundings, during their life span. In the case of the SLD, although the local alongshore winds may not be favorable for coastal upwelling, cooler, nutrient rich water is brought to the surface by open ocean upwelling within the dome. The importance of the dome is apparent and its predictability should be useful for coastal oceanographic applications. This study further demonstrates that it is necessary to take into account the effects of local winds as well as remote forcing to understand the dynamics of circulation in this region, as in the previous investigations (MKM; MHSS; Vinayachandran et al. 1996).

The study provides further insight into the structure of the SMC. As in MKM, part of the SMC turns northeastward east of Sri Lanka and flows into the Bay of Bengal. This turning, the shallow nature of the SMC, and its termination in the east are attributed to Rossby wave propagation. The Rossby wave associated with the spring Wyrtki (1973) jet has dominant velocity toward the northeast. A second Rossby wave, generated by weakening of the spring Wyrtki jet and wind stress curl in the eastern Bay of Bengal, has dominant velocity toward the southwest. We note that, while both Rossby waves can cause the migration of the SMC toward the coast of Sri Lanka and maintain the northeastward branch that flows into the Bay of Bengal, it is the second Rossby wave that cause the termination of the eastern branch and the observed shallow nature of the SMC (Schott et al. 1994).

We have shown, for the first time, that anticyclonic vortices formed due to the barotropic instability are embedded in the circulation in this region. While its close location to the equator causes the dynamics of the anticyclonic vortex south of Sri Lanka to be predominantly planetary geostrophic, the eddy east of the SLD is in intermediate geostrophic balance. The anticyclonic vortex in the SMC is supported by satellite altimetry whereas the eddy east of the SLD lacks observational evidence despite its robust dynamics. Future in situ observational programs should provide a three-dimensional structure as well as verify the existence of these unique vortices.

Schott et al. (1994) suggested that the crucial link that connects the Bay of Bengal and the rest of the Indian Ocean could be the coastal circulation around Sri Lanka. The ship drifts (Cutler and Swallow 1984), which are the only observational evidence for the flow around the Indian subcontinent and Sri Lanka, and the present model results suggest that an uninterrupted current around India and Sri Lanka is present only during the November–January period. During the SWM the southern part of the EICC is often northward (Shetye et al. 1991), suggesting that a link via the coastal circulation during the SWM is unlikely. A possible link that connects the Bay of Bengal with the rest of the Indian Ocean during the SWM is that part of the SMC that turns northeastward and flows into the Bay

Though the present model can reproduce many features of the observed seasonal cycle of the circulation in the Indian Ocean, it has two obvious limitations. First, the simulated upper-layer temperature is too cool. Second, the model does not take into account salinity variations that could have a significant role in the coastal circulation around India and Sri Lanka. Both are tractable to some extent using better parameterization of the mixed layer as well as high quality data and efforts in this direction are under way.

Acknowledgments

We thank Yukio Masumoto and Takashi Kagimoto for their help in running the model on the Hitachi supercomputer of the University of Tokyo. Comments by Dr. Julian McCreary and two anonymous referees greatly helped in improving the manuscript. We are thankful to Dr. D. P. Chambers for providing the T/P data and Drs. R. Lukas, H. Nakamura, and Y. Wakata for useful discussions. This study was supported by the Japan Ministry of Education, Science and Culture under contracts of the Grant-in-Aid for General Scientific Research (06452085) and the International Scientific Research Program (05044034).

REFERENCES

Boning, C. W., and R. G. Budich, 1992: Eddy dynamics in a primitive equation model: Sensitivity to horizontal resolution and friction. *J.*

Phys. Oceanogr., **22,** 361–381..

Cox, M. D., 1984: A primitive equation 3-dimensional model of the ocean. GFDL/NOAA Tech. Rep. 1, GFDL/NOAA, Princeton University Press, Princeton, NJ, 250 pp..

Cutler, A. N., and J. C. Swallow, 1984: Surface currents of the Indian Ocean (to 25°S, 100°E). Compiled from historical data archived by the Meteorological Office, Bracknel, UK, Rep. 187, Institute of Oceanographic Sciences, Wormley, UK. 8 pp. and 36 charts..

Greatbatch, R. J., 1985: Kelvin wave fronts, Rossby solitary waves and nonlinear spin-up of the equatorial oceans. *J. Geophys. Res.*, **90,** 9097–9107..

Hastenrath, S., and L. Greischar, 1991: The monsoonal current regimes of the tropical Indian Ocean: Observed surface flow fields and their geostrophic and wind-driven components. *J. Geophys. Res.*, **96,** 12 619–12 633..

Hellerman, S., and M. Rosenstein, 1983: Normal monthly wind stress over the world ocean with error estimates. *J. Phys. Oceanogr.*, **13,** 1093–1104..

Legeckis, R., 1987: Satellite observations of a western boundary current in the Bay of Bengal. *J. Geophys. Res.*, **92,** 12 974–12 978..

Levitus, S., 1982: *Climatological Atlas of the World Ocean.* NOAA Prof. Paper No. 13, U.S. Govt. Printing Office, 173 pp..

— , and T. P. Boyer, 1994: *World Ocean Atlas.* Vol. 4: *Temperature,* NOAA Atlas NESDIS 4, U.S. Govt. Printing Office 117 pp..

— , R. Burgett, and T. P. Boyer, 1994: *World Ocean Atlas.* Vol. 5: *Salinity.* NOAA Atlas NESDIS 3, U.S. Govt. Printing Office, 99 pp..

Masumoto, Y., and T. Yamagata, 1991: Response of the tropical Pacific to the Asian winter monsoon: The generation of the Mindanao dome. *J. Phys. Oceanogr.*, **21,** 1386–1398..

— , and — , 1993: Simulated seasonal circulation in the Indonesian Seas. *J. Geophys. Res.*, **98,** 12 501–12 509..

— , and — , 1996: Seasonal variations of the Indonesian throughflow in a general ocean circulation model. *J. Geophys. Res.*, **101,** 12 287–12 293..

McCreary, J. P., P. K. Kundu, and R. L. Molinari, 1993: A numerical investigation of the dynamics, thermodynamics and mixed-layer processes in the Indian Ocean. *Progress in Oceanography*, Vol. 31, Pergamon, 181–224..

— , W. Han, D. Shankar, and S. R. Shetye, 1996: Dynamics of the east India coastal current. 2. Numerical solutions. *J. Geophys. Res.*, **101,** 13 993–14 010..

Murthy, V. S. N., Y. V. B. Sarma, D. P. Rao, and C. S. Murthy, 1992:Water characteristics, mixing and circulation in the Bay of Bengal during southwest monsoon. *J. Mar. Res.*, **50,** 207–228..

Oberhuber, J. M., 1988: *An Atlas Based on COADS Data Set: The Budget of Heat, Buoyancy and turbulent Kinetic Energy at the Surface of the Global Ocean.* MPI Rep. 15, Max Planck Institute for Meteorology, Hamburg, Germany, 100 pp.

Pacanowski, R. C., and S. G. H. Philander, 1981: Parameterization of vertical mixing in numerical models of the tropical ocean. *J. Phys. Oceanogr.*, **11,** 1442–1451..

Potemra, J. T., M. E. Luther, and J. J. O'Brien, 1991: The seasonal circulation of the upper ocean in the Bay of Bengal. *J. Geophys. Res.*, **96,** 12 667–12 683..

Schott, F., J. Reppin, and J. Fischer, 1994: Currents and transports of the monsoon current south of Sri Lanka. *J. Geophys. Res.*, **99,** 25 127–25 141..

Shankar, D., J. P. McCreary, W. Han, and S. R. Shetye, 1996: Dynamics of the east India coastal current. 1. Analytical solutions forced by interior Ekman pumping and local alongshore winds. *J. Geophys. Res.*, **101,** 13 975–13 991..

Shetye, S. R., S. S. C. Shenoi, A. D. Gouveia, G. S. Michael, D. Sundar, and G. Nampoothiri, 1991: Wind-driven coastal upwelling along the western boundary of the Bay of Bengal during the southwest monsoon. *Contin. Shelf Res.*, **11,** 1397–1408..

— , A. D. Gouveia, S. S. C. Shenoi, D. Sundar, G. S. Michael, and G. Nampoothiri, 1993: The western boundary current of the seasonal subtropical gyre in the Bay of Bengal. *J. Geophys. Res.*, **98,** 945–954..

— , — , D. Shankar, S. S. C. Shenoi, P. N. Vinayachandran, D. Sundar, G. S. Michael, and G. Nampoothiri, 1996: Hydrography and circulation in the western Bay of Bengal during the Northeast Monsoon. *J. Geophys. Res.*, **101,** 14 011–14 025..

Stockdale, T., D. Anderson, M. Davey, P. Delelcluse, A. Kattenberg, Y. Kitamura, M. Latif, and T. Yamagata, 1993: Inter-comparison of tropical ocean GCMs, Publ. WCRP-79, WMO/TD 545, World Clim. Res. Program, WMO, Geneva, 90 pp..

Suryanarayana, A., V. S. N. Murthy, and D. P. Rao, 1993: Hydrography and circulation of the Bay of Bengal during early winter, 1983. *Deep-Sea Res.*, **40,** 205–217..

Tapley, B. D., D. P. Chambers, C. K. Shum, R. J. Eanes, J. C. Ries, and R. H. Stewart, 1994: Accuracy assessment of the large-scale dynamic ocean topography from TOPEX/POSEIDON altimetry. *J. Geophys. Res.*, **99,** 24 605–24 617..

Umatani, S., and T. Yamagata, 1991: Response of the eastern tropical Pacific to meridional migration of the ITCZ: The generation of the Costa Rica dome. *J. Phys. Oceanogr.*, **21,** 346–363..

Vinayachandran, P. N., S. R. Shetye, D. Sengupta, and S. Gadgil, 1996: Forcing mechanisms of the Bay of Bengal circulation. *Curr. Sci.*, **71,** 753–763..

Williams, G. P., and T. Yamagata, 1984: Geostrophic regimes, intermediate solitary vortices and Jovian eddies. *J. Atmos. Sci.*, **41,** 453–478.. Find this article online

— ~~,~~and R. J. Wilson, 1988: The stability and genesis of Rossby vortices. *J. Atmos. Sci.*, **45,** 207–241.. Find this article online

Wyrtki, K., 1973: An equatorial jet in the Indian Ocean. *Science,* **181,** 262–264..

Yamagata, T., 1982: On nonlinear planetary waves: A class of solutions missed by the traditional quasi-geostrophic approximation. *J. Oceanogr. Soc. Japan*, **38,** 236–244..

— ~~,~~and S. Iizuka, 1995: Simulation of the tropical thermal domes in the Atlantic: A seasonal cycle. *J. Phys. Oceanogr.*, **25,** 2129–2140..

Yu, L., J. J. O'Brien, and J. Yang, 1991: On the remote forcing of the circulation in the Bay of Bengal. *J. Geophys. Res.*, **96,** 20 449–20 454..

Figures

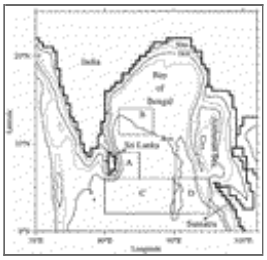

Click on thumbnail for full-sized image.

Fig. 1. Geometry of the coastline and bottom topography of the study area in the model. Thick line represents the land boundary in the model. Contours are isobaths. Dashed contours are for 200 m and 2 km. Boxes A, B, C, and D have reference to Figs. 8, 12, and 18.

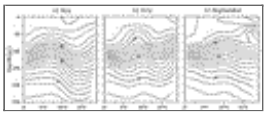

Click on thumbnail for full-sized image.

Fig. 2. Vertical section of climatological temperature (Levitus and Boyer 1994) along 85°E for the months of (a) May, (b) July, and (c) September. Contour interval is 1°C. Every fifth contour is marked by a thick line.

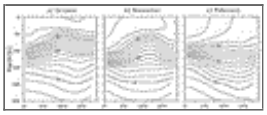

Click on thumbnail for full-sized image.

Fig. 3. Vertical section of climatological temperature (Levitus and Boyer 1994) along 85°E for the months of (a) October, (b) December, and (c) February. Contour interval is 1°C. Every fifth contour is marked by a thick line.

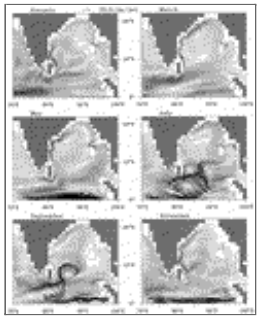

Click on thumbnail for full-sized image.

Fig. 4. Bimonthly maps of currents from the model at a depth of 35 m.

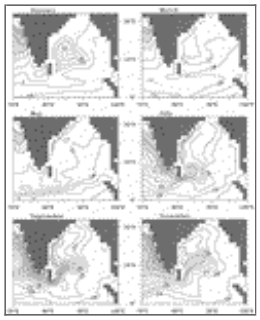

Click on thumbnail for full-sized image.

Fig. 5. Bimonthly maps of temperature from the model at a depth of 35 m. Contour interval is 1°C. Regions with temperature less than 25°C are shaded.

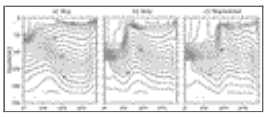

Click on thumbnail for full-sized image.

Fig. 6. Vertical section of temperature from the model, along 85°E for the months of (a) May, (b) July, and (c) September. Contour interval is 1°C. Every fifth contour is marked by a thick line.

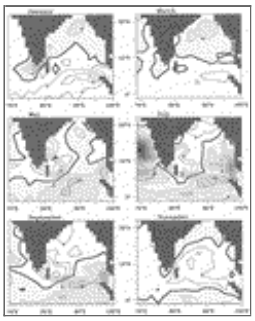

Click on thumbnail for full-sized image.

Fig. 7. Bimonthly maps of curl of the wind stress (Hellerman and Rosenstein 1983). Contour interval is 5×10^{-9} dyn cm^{-3}. Negative values are shaded. Note the strong cyclonic (anticlockwise) curl east of Sri Lanka and the strong anticyclonic (clockwise) curl near the eastern boundary during the southwest monsoon.

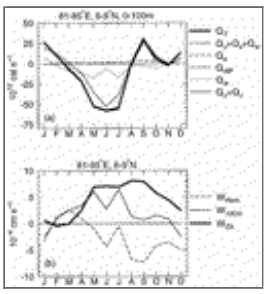

Click on thumbnail for full-sized image.

Fig. 8. (a) Heat balance analysis for the Sri Lanka dome. The dimensions of the box chosen (box A in Fig. 1) are shown at the top of the figure. The rate of change of heat storage (Q_T) is given by $Q_T = Q_u + Q_v + Q_w + Q_s + Q_{diff}$, where Q_u, Q_v, and Q_w are net zonal, meridional, and vertical fluxes; Q_s is the heat flux from the atmosphere; and Q_{diff} is the contribution from diffusive processes. (b) Vertical velocity at 107 m from the model (thin continuous line), Ekman pumping velocity (thick line), and the upwelling due to remote effects (dashed line). Remote upwelling is calculated as the difference between the model vertical velocity and Ekman pumping. All values are averaged over the horizontal region shown above the figure.

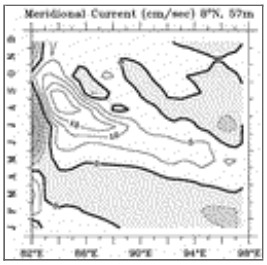

Click on thumbnail for full-sized image.

Fig. 9. Time–longitude section of meridional velocity from the model, at a depth of 57 m along 8°N. Contour interval is 5 cm s^{-1}. Regions with southward flow is shaded as well as shown by dashed contours. A Rossby wave signal radiating from the eastern boundary during April–June hits the east coast of Sri Lanka during September.

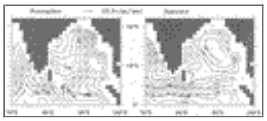

Click on thumbnail for full-sized image.

Fig. 10. Dynamic topography of the sea surface with reference to 500 m calculated from the climatological (Levitus and Boyer 1994; Levitus et al. 1994) data for the months of November (left panel) and January (right panel). Contour interval is 2 dyn cm. Arrows represent geostrophic currents.

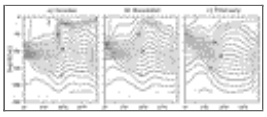

Click on thumbnail for full-sized image.

Fig. 11. Vertical section of temperature from the model, along 85°E for the months of (a) October, (b) December, and (c) February. Contour interval is 1°C. Every fifth contour is marked by a thick line.

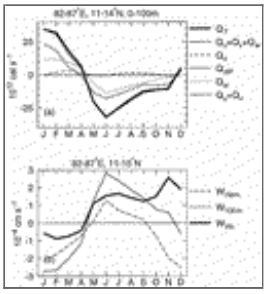

Click on thumbnail for full-sized image.

Fig. 12. As in Fig. 8 but for the Bay of Bengal dome, for the region shown by box B in Fig. 1.

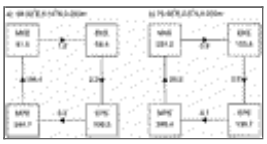

Click on thumbnail for full-sized image.

Fig. 13. Values of the energy components ($cm^2\ s^{-2}$) and interaction terms ($10^{-5}\ cm^2\ s^{-3}$) for (a) the IG eddy east of the SLD and (b) for the anticyclonic vortex south of Sri Lanka. All terms calculated for the boxes are shown above the figures using the formulas given by Boning and Budich (1992). See text for acronyms.

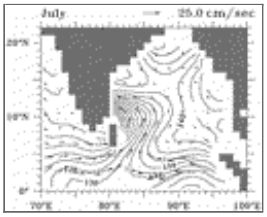

Click on thumbnail for full-sized image.

Fig. 14. As in Fig. 10 but for the month of July.

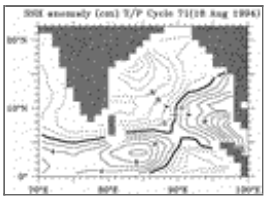

Click on thumbnail for full-sized image.

Fig. 15. Sea surface height (SSH) anomaly from TOPEX/Poseidon altimeter. The anomaly is defined as the difference from the mean SSH for the period November 1992–November 1996 (Tapley et al. 1994). Contour interval is 2 cm and negative anomalies are shown by dashed contours.

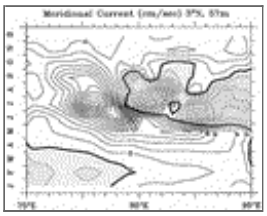

Click on thumbnail for full-sized image.

Fig. 16. Time–longitude section of meridional velocity from the model, at a depth of 57 m along 3°N. Contour interval is 2 cm s^{-1}. Regions with southward flow are shaded as well as shown by dashed contours.

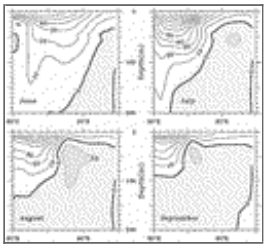

Click on thumbnail for full-sized image.

Fig. 17. Vertical section of zonal velocity along 5°N, during the SWM. Contour interval is 10 cm s^{-1}. Thick contour represents zero. Westward flow is shaded as well as shown by dashed contours. Note the westward propagation of westward flow and the consequent reduction in thickness of the layer with eastward flow.

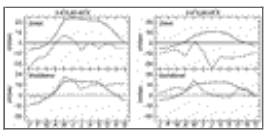

Click on thumbnail for full-sized image.

Fig. 18. Ekman (full line) and geostrophic (dashed) components of surface flow. Ekman components are calculated from the Hellerman and Rosenstein (1983) wind stress values using the formula used by Hastenrath and Greischar (1991). Geostrophic currents are calculated from dynamic heights (with reference to 500 m) based on climatological temperature (Levitus and Boyer 1994) and salinity (Levitus et al. 1994). Average values for the box C (Fig. 1) are shown in the left panel and that for box D (Fig. 1) are shown in the right panel.

* Current affiliation: Institute for Global Change Research, Minato-ku, Tokyo, Japan.

Corresponding author address: Prof. Toshio Yamagata, Department of Earth and Planetary Physics, Graduate School of Science, University of Tokyo, Hongo 7-3-1, Bunkyo-ku, Tokyo 113, Japan.

E-mail: yamagata@geoph.s.u-tokyo.ac.jp

top